Journal of Colloid and Interface Science 622 (2022) 419–430

Contents lists available at ScienceDirect

Journal of Colloid and Interface Science

journal homepage: www.elsevier.com/locate/jcis

Uncoupling bacterial attachment on and detachment from polydimethylsiloxane surfaces through empirical and simulation studies

Fei Pan [a,1], Mengdi Liu [a,b,1], Stefanie Altenried [a], Min Lei [c], Jiaxin Yang [d], Hervé Straub [a], Wolfgang W. Schmahl [b], Katharina Maniura-Weber [a], Orane Guillaume-Gentil [e], Qun Ren [a,*]

[a] Laboratory for Biointerfaces, Empa, Swiss Federal Laboratories for Materials Science and Technology, Lerchenfeldstrasse 5, 9014 St. Gallen, Switzerland
[b] Department of Earth- and Environmental Sciences, Ludwig Maximilian University of Munich, Theresienstrasse 41, 80333 Munich, Germany
[c] College of Textiles, Donghua University, North Renmin Road 2999, 201620 Shanghai, China
[d] Key Laboratory of Rare Earth Resource Utilization, Changchun Institute of Applied Chemistry, CAS, 130022 Changchun, China
[e] Institute of Microbiology, Department of Biology, ETH Zurich, Vladimir-Prelog-Weg 4, 8093 Zurich, Switzerland

GRAPHICAL ABSTRACT

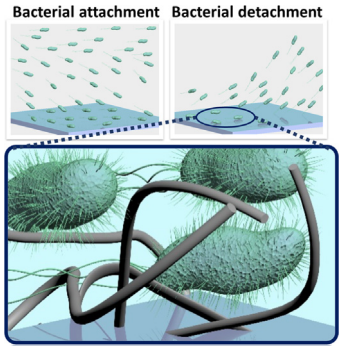

ARTICLE INFO

Article history:
Received 10 February 2022
Revised 10 March 2022
Accepted 13 April 2022
Available online 16 April 2022

Keywords:
Bacterial attachment and detachment
PDMS
Mechanical property
Interfacial physicochemistry
XDLVO
Burst/sublayer modelling
Single cell adhesion spectroscopy

ABSTRACT

Bacterial infections related to medical devices can cause severe problems, whose solution requires in-depth understanding of the interactions between bacteria and surfaces. This work investigates the influence of surface physicochemistry on bacterial attachment and detachment under flow through both empirical and simulation studies. We employed polydimethylsiloxane (PDMS) substrates having different degrees of crosslinking as the model material and the extended Derjaguin – Landau – Verwey – Overbeek model as the simulation method. Experimentally, the different PDMS materials led to similar numbers of attached bacteria, which can be rationalized by the identical energy barriers simulated between bacteria and the different materials. However, different numbers of residual bacteria after detachment were observed, which was suggested by simulation that the detachment process is determined by the interfacial physicochemistry rather than the mechanical property of a material. This finding is further supported by analyzing the bacteria detachment from PDMS substrates from which non-crosslinked polymer chains had been removed: similar numbers of residual bacteria were found on the

* Corresponding author.
E-mail address: Qun.Ren@empa.ch (Q. Ren).
[1] These authors contributed equally.

https://doi.org/10.1016/j.jcis.2022.04.084

FluidFM

extracted PDMS substrates. The knowledge gained in this work can facilitate the projection of bacterial colonization on a given surface.

1. Introduction

Material properties, including mechanical parameters, are well known to impact bacterial interactions with materials [1-4]. It has been reported that stiffness of substrate materials can significantly influence bacterial adhesion [5-9], e.g. *Escherichia coli*, *Staphylococcus aureus*, *Pseudoalteromonas* sp. and *Bacillus* sp. displayed a higher number of adhering bacteria on stiff than on soft materials such as agarose, agar and poly(ethylene glycol) dimethacrylate (PEGDMA) hydrogels [9-11]. Recently, we revealed that the intrinsic properties of polydimethylsiloxane (PDMS) substrates of different Young's moduli substantially impacted bacterial adhesion, in addition to the reported bacterial active mechanosensing [12]. Moreover, the material viscosity, as we discovered, strongly influences the irreversible adhesion of *E. coli* on PDMS surfaces [13]. The higher viscosity of soft PDMS surfaces led to a higher number of adhered *E. coli* cells, likely due to higher stickiness and/or deformability of the soft PDMS surface [13]. We further found that the interfacial chemical properties played a critical role in bacterial adhesion by effectively influencing the material interfacial viscosity instead of material mechanical properties [1].

Since bacterial adhesion to surfaces mostly takes place under flow conditions, e.g. in the environment of dental implants, urinary catheter and stents, and wound dressings, it is important to understand how bacteria interact with material surfaces under flow and to discover the influencing factors. To this end, mathematical simulations were proposed to explain and predict the interaction between bacteria and material surfaces. The extended Derjaguin – Landau – Verwey – Overbeek (XDLVO) model has been developed by involving Lewis acid – base interaction in addition to Coulomb and Van der Waals interactions [14]. The XDLVO model has been used to simulate the free energy between a bacterium and a flat surface by assuming a bacterium as a homogeneous spherical particle and neglecting the influence of its appendages [15]. It was revealed that the bond between a substratum surface and a bacterium becomes stronger after initial attachment [15]. In addition, the burst/sublayer model has been exploited to calculate the critical shear velocity to detach bacteria from a surface and to analyze the residual resistant torques of different PDMS surfaces by considering the turbulences of the fluids [16,17]. Briefly explained, the burst method was applied to PDMS surfaces in the high fluid turbulence scenario ($1 \leq Re \leq 1000$) and the sublayer method was in the low fluid turbulence regime ($Re \ll 1$) [16,18]. However, in the models reported so far the processes of attachment and detachment are not lucidly separated and studied regarding the influence of shear velocity, residual resistant torques, and fluid turbulences on bacterial attachment and detachment.

The goal of this work is to decouple and differentiate the bacterial attachment from their detachment process, and furthermore to discover what causes the numerical difference of bacteria on PDMS surfaces during attachment and after detachment. Herein we separate bacterial attachment and detachment into two separate phases. Bacterial attachment has been considered as reversible adhesion and the residual cell attachment after detachment as irreversible adhesion. Bacterial cells were idealized as microparticles (Fig. 1a) for XDLVO model simulations during the attachment process to study the effects of the adhesion energy barrier on bacterial attachment. The burst/sublayer model was utilized for the bacterial detachment process to calculate critical shear forces on different PDMS surfaces and residual resistant torques, which qualitatively depicted the properties of different PDMS surfaces during the detachment process. A fluidic force microscope (FluidFM), capable of measuring a single cell adhesion force on surfaces [19,20], was utilized to quantify the adhesion force between a bacterium and a surface. It was revealed that the simulation results for the attachment and detachment process correlated well with those obtained experimentally (Fig. 1b-e), both of which suggest that the number of residual bacteria on the surface is determined by interfacial physicochemistry in the detachment process. This work allows an improved understanding of how bacteria interact with viscoelastic surfaces involving attachment and detachment processes under flow conditions.

2. Results and discussion

2.1. Physicochemical characterization of PDMS surfaces

In this work, we used different PDMS samples as described previously [1]. The bulk PDMS properties were characterized by rheology and the results are shown in Fig. S1 & Table 1. Similarly to our previous report [1], PDMS species with 5:1, 10:1, 20:1 and 40:1 ratios of elastomer and curing agent showed decreasing complex shear moduli but an increasing viscosity. The adhesion force and the adhesion energy of bulk PDMS increased with decreasing crosslinking degree. Furthermore, the gel fraction analysis revealed that there was an increasing amount of free PDMS polymer chains inside PDMS with decreasing crosslinking degree, contributing to the high viscosity of the soft PDMS species. Decreasing crosslinking degree led to decreased Young's moduli but increased maximum adhesion forces on PDMS surfaces, as well as slightly higher water contact angle (Fig. S2). Slightly different roughness (Rq) of the four PDMS samples was measured (Fig. S2), indicating that the different amount of free PDMS polymer chains inside the PDMS samples did not dramatically affect surface roughness.

2.2. PDMS of different viscoelasticity allowed similar numbers of initially attached bacteria

When bacteria were perfused for two hours in a flow chamber, similar numbers of attached bacteria were found on the distinct PDMS surfaces having different stiffness, namely 11101 ± 680, 11586 ± 752, 11493 ± 768, and 11470 ± 550 cells·mm^{-2} on PDMS 5:1, 10:1, 20:1 and 40:1, respectively (Fig. 2 a&b). These results opposed those previously reported, where more adhered bacteria were observed on soft PDMS surfaces under static conditions [1,12]. We attribute this difference to the different experimental procedure: under the static condition bacteria on PDMS surfaces were counted after removal of the bacterial suspension and rinsing the loosely attached bacteria, a procedure during which air–liquid interfaces can wash off some attached bacteria [21], thus resulting in variation of the adhered cell numbers. In contrast, under the flow condition applied here, the bacteria on PDMS surfaces during the attachment process were directly counted without prior removal or rinsing.

To simulate the interaction between floating bacteria and PDMS surfaces, we performed theoretical modelling using the extended Derjaguin – Landau – Verwey – Overbeek (XDLVO) model, which

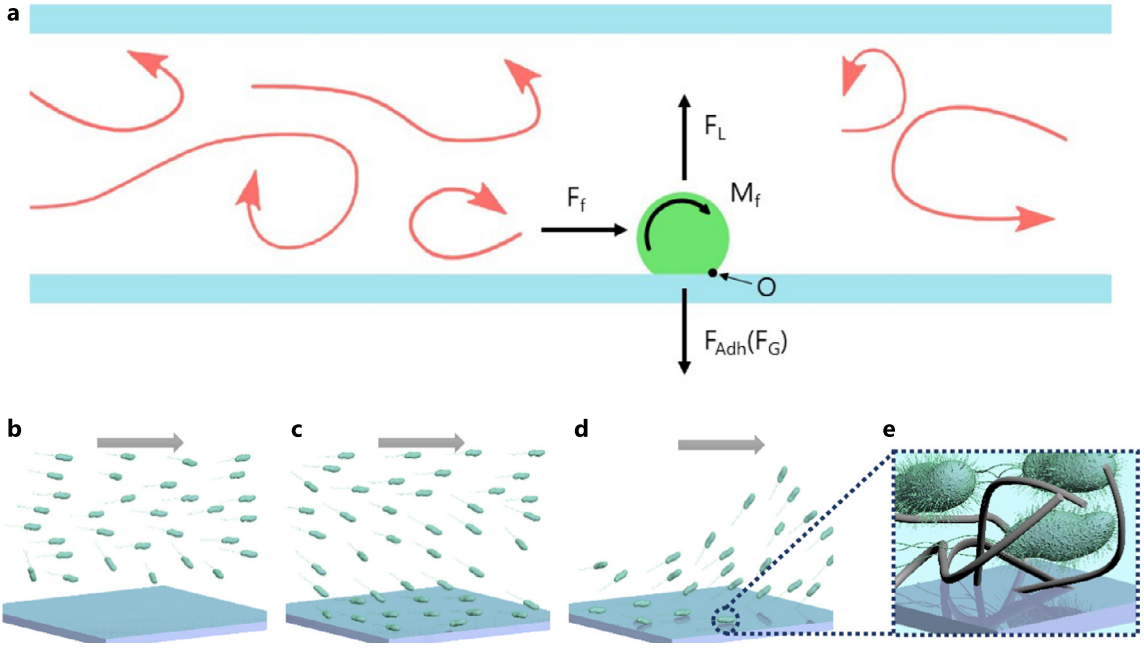

Fig. 1. Scheme of bacterial interaction with surfaces. Bacteria rolling detachment (a) in a flowing chamber. F_f is the hydrodynamic force exerted by the flow; M_f is the hydrodynamic momentum; F_{adh} is the adhesion force based on JKR model; the F_L (lift force) and F_G (gravity force) are neglected in this work due to their limited contribution [17]; the detachment model was based on the torque equilibrium theory around point "O". The red colored arrows represent the bacterial movement under flow. Illustration of bacterial movements on PDMS surfaces of different stiffness during (b) initial perfusion, (c) bacterial attachment and (d) bacterial detachment. Interaction of residual bacteria with PDMS surface is depicted in (e). Similar numbers of adhered bacteria were found on PDMS surfaces of different stiffness during (c) bacterial attachment and different numbers of residual bacteria adhered on different PDMS surfaces after (d) bacterial detachment. It is hypothesized that the surface physicochemistry of different PDMS surfaces, namely the free polymer chains and polymer chain ends (grey filaments in (e)), is the critical factor to influence the residual bacterial adhesion. The grey arrow bar indicated the flow direction of bacterial suspension (b & c) and PBS buffer or air (d). (For interpretation of the references to colour in this figure legend, the reader is referred to the web version of this article.)

Table 1
Rheological properties of non-extracted and extracted PDMS. The storage modulus, loss modulus and loss factor were measured by a rheometer in the linear viscoelastic region as reported [1] with the time-sweep mode, and the shear complex modulus was subsequently derived based on the formula described in the Methods. The shear complex modulus as noted rose with the increasing crosslinking degree for both non-extracted and extracted PDMS samples, although the extracted counter samples displayed higher modulus. The loss factor, the numerical ratio of loss modulus over storage modulus, suggested that the non-extracted and extracted PDMS samples of lower crosslinking degree possess a high viscosity and low elasticity. Three independent measurements were performed with three replicates for one sample in one measurement. Standard deviations were derived according to 9 analyses of one sample.

PDMS Species	Shear Modulus (G*)/kPa	Storage Modulus (G')/kPa	Loss Modulus (G")/kPa	Loss factor	Extraction
5: 1	69.0 ± 0.22	68.9 ± 0.22	3.4 ± 0.21	0.049 ± 0.001	No
	7385.6 ± 142.12	7370.8 ± 142.09	478.5 ± 14.02	0.064 ± 0.003	Yes
10: 1	52.7 ± 0.43	52.6 ± 0.43	2.8 ± 0.11	0.052 ± 0.001	No
	4186.9 ± 8.22	4176.1 ± 8.03	286.7 ± 2.13	0.068 ± 0.004	Yes
20: 1	41.2 ± 0.09	41.2 ± 0.09	1.9 ± 0.03	0.046 ± 0.001	No
	4014.9 ± 9.45	3999.1 ± 9.35	355.6 ± 1.63	0.089 ± 0.002	Yes
40: 1	4.3 ± 0.05	4.2 ± 0.05	1.1 ± 0.02	0.258 ± 0.001	No
	2422.5 ± 14.01	2360.5 ± 13.65	544.6 ± 4.02	0.231 ± 0.003	Yes

has been exploited to describe the interaction between a bacterial cell and a material surface in colloidal physics, by assuming bacterial cells as homogeneous spherical particles and neglecting the cell surface appendages [22,23]. The XDLVO model considers acid-base interaction, the electrostatic double layer interaction, and the Lifshitz-Van der Waals interaction for calculation of free energy. In the experimental settings, the total free energy in the DLVO model between a surface and a particle is the sum of their Coulomb and Van der Waals interactions, in which the electrostatic Coulomb interaction is repulsive due to the negative surface charge of a bacterium and the negatively charged PDMS surface in a neutral aqueous solution. This repulsive energy increases as the ionic strength decreases because of a weaker charge shielding effect of ions in the electrical double layer. The Debye length of the PBS buffer utilized in our experiment and simulation was 0.787 nm. The electrostatic potential would decay to 2% of its value at the surface when exceeding the region of varying electrostatic potential within a distance of about 3 times the Debye length [14]. The short-ranged competing attractive Van der Waals force dominates the vicinity of a surface within several nanometers [14]. Thereby, the Coulomb interaction and Van der Waals force lead to a shallow secondary energy minimum and an energy barrier, for which bacterial cells do not compensate by Brownian motion [24]. Additionally, Lewis acid-base interaction energy had to be considered here [25,26]. The decrease of the energy barrier and deeper secondary energy minimum was consequently taken into consideration for the calculation of the interaction gap influenced by the strong short-ranged Lewis acid-base interaction. The calculated gap required for the interaction between bacteria and PDMS surfaces of different interfacial Young's moduli was 4 nm within the reported distance [27] (Fig. 2c). The calculated free energy of the interaction between bacterium and different PDMS surfaces derived the same energy bar-

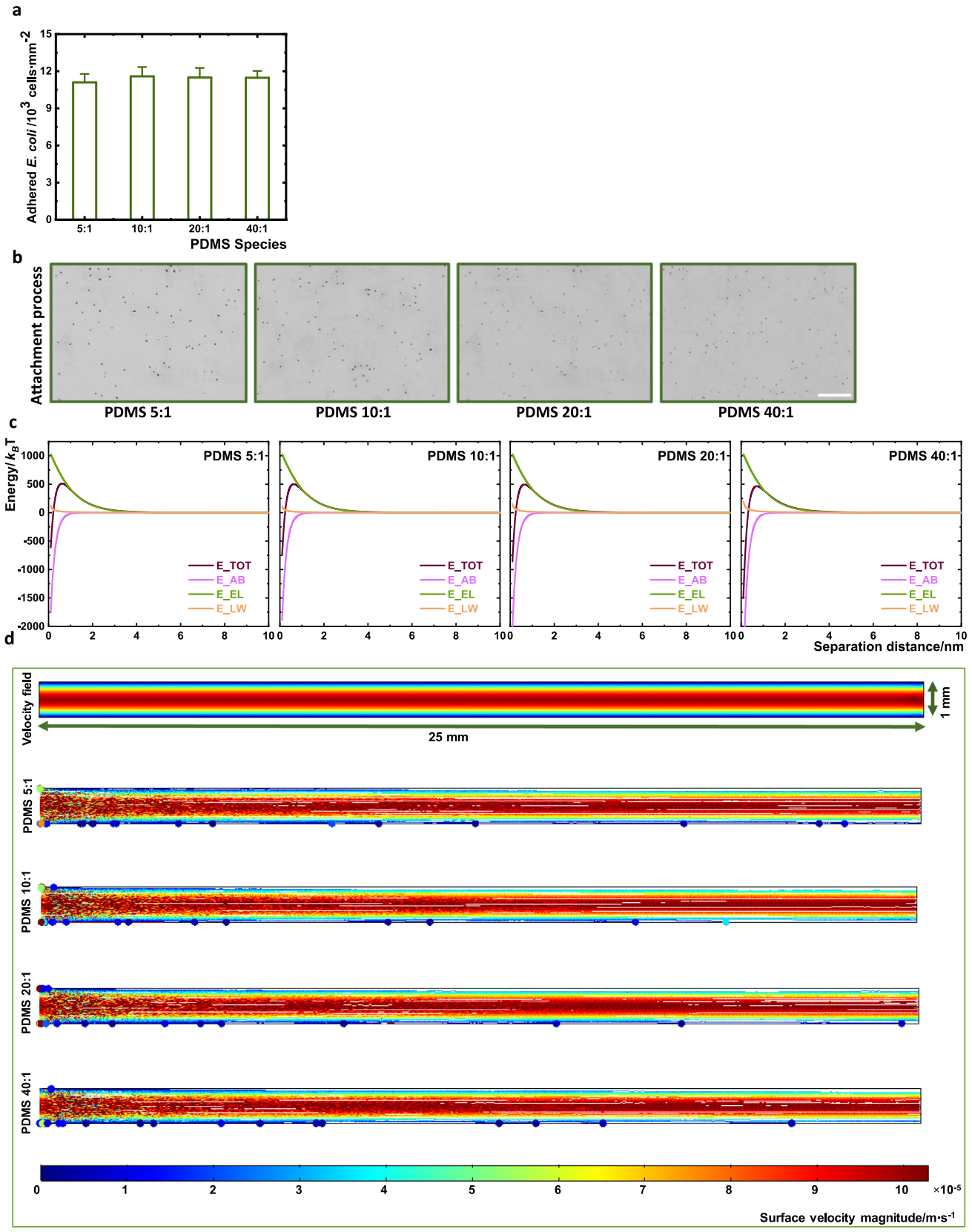
a
Adhered E. coli /10^3 cells·mm^-2
PDMS Species
5:1
10:1
20:1
40:1
b
Attachment process
PDMS 5:1
PDMS 10:1
PDMS 20:1
PDMS 40:1
c
Energy/ k_BT
E_TOT
E_AB
E_EL
E_LW
Separation distance/nm
d
Velocity field
25 mm
1 mm
PDMS 5:1
PDMS 10:1
PDMS 20:1
PDMS 40:1
×10^-5
Surface velocity magnitude/m·s^-1

rier of 500 k_BT for bacterial interaction on different PDMS surfaces, appearing at a similar distance of 0.6 nm for all samples, smaller than 4 nm (Fig. 2c).

Further, to study bacterial adhesion on PDMS surfaces during the attachment process, laminar flow was exploited to create a flowing system in a 2D cross-section construction, identical to the experimental settings. Particle tracing in fluid flow was utilized in the simulation to understand simulated bacteria attachment behavior on different PDMS surfaces, where the flowing particles were set as 0.3 mg·s^{-1} analogous to the concentration of bacteria in the flow. Consequently, the particles, simulated at the same flow conditions as used in the experiments, adhered in roughly comparable numbers ($\sim$ 90 particles) on the cross-sections of different PDMS material surfaces (Fig. 2d). This theoretical explanation of similar numbers of bacterial attachment on different PDMS surfaces suggests that the bacterial adhesion during the attachment process is a non-specific process and not influenced by specific factors e.g. bacterial mechano-sensing. The similar energy barrier of different PDMS surfaces is the main reason for the comparable bacterial adhesion during the bacterial attachment process.

2.3. PDMS of different interfacial viscoelasticity allowed different numbers of residual bacteria after detachment

A detachment process was applied to flush away the loosely attached bacteria on the sample surfaces, as described previously [13]. The numbers of residual bacteria varied dramatically on different PDMS surfaces with more residual bacteria on lower crosslinked PDMS surfaces: 1200 ± 113, 2908 ± 463, 6093 ± 826, 9462 ± 1459 cells·mm^{-2} on PDMS 5:1, 10:1, 20:1 and 40:1, respectively (Fig. 3a&b). The different numbers of residual bacteria adhered on different PDMS surfaces motivated us to unveil the influential factors by using a theoretical simulation. A bacterium was assumed as an elastic spherical particle interacting with a sample surface of a much smaller roughness compared to the particle radius [28]. To detach an attached spherical particle from a surface, it is required that the torque of the flow should be larger than that generated by the particle-interface adhesion force and the weight of the particle. The required minimum flowing torque was named critical torque, generating a respective critical shear velocity [17]. We calculated the residual numbers of bacteria on different PDMS surfaces after the detachment procedure using the burst/sublayer method [16,17] by exploiting the JKR (Johnson, Kendall and Roberts) adhesion model [29], a hydrodynamic model [30] and Monte-Carlo simulation [31] (Fig. 1a). Here the JKR adhesion model incorporated the dominant contribution from the adhesion force when the simulated bacterium contacts PDMS surfaces. The hydrodynamic model considered critical shear velocity of the flow and the critical torque to flush away the simulated attached bacterium on the PDMS surfaces. Assisted with Monte-Carlo simulation, we investigated the distribution of critical shear velocity and the numerical relation between shear velocity and the detached bacteria from a surface due to the imperfect interfacial homogeneity, unequal bacterial distribution and flow variation. Furthermore, we derived the distribution of resistant torque necessary to be overcome by a flow for a successful detachment of a bacterium from a given surface. Based on calculation assumptions and dependence on Reynolds (Re) number, the burst method was applicable for PDMS surfaces in the high fluid turbulence scenario ($1 \leq Re \leq 1000$) and the sublayer method in low fluid turbulence regimes ($Re \ll 1$) [16,18]. Thereby, the critical shear velocities (u*) to detach a simulated bacterium from PDMS 5:1 and PDMS 10:1 were derived as 1.0 m·s^{-1} and 1.44 m·s^{-1} with the sublayer method, and those for PDMS 20:1 and 40:1 were calculated with the burst method as u^*_{min} 9.36 m·s^{-1} and u^*_{max} 9.69 m·s^{-1} for PDMS 20:1 and u^*_{min} 20.83 m·s^{-1} and u^*_{max} 21.56 m·s^{-1} for PDMS 40:1, respectively (Fig. 3c). Although we cannot derive a specific critical velocity to detach a bacterium on PDMS 20:1 and 40:1, it can be noticed that the critical velocities increased with decreasing crosslinking degrees of the samples. Similarly, the residual resistant torques increased as well with decreasing crosslinking degree, with PDMS 5:1, 10:1, 20:1 and 40:1 at 1.70×10^{-18} N·m, 3.08×10^{-18} N·m, 2.09×10^{-16} N·m, 5.98×10^{-16} N·m, respectively. Considering inhomogeneous distribution of bacteria and variation of flow conditions on the inhomogeneous PDMS surfaces, we concluded that the bacterial attachment on surfaces impacted by detachment cannot be compensated by the flow (Fig. 3d and S3). A numerical relation between flow shear velocity and detached bacterial numbers demonstrated that detaching 50% bacteria from different PDMS surfaces required shear velocities of 1.0 m·s^{-1}, 1.45 m·s^{-1}, 9.59 m·s^{-1} and 22.42 m·s^{-1} for PDMS 5:1, 10:1, 20:1 and 40:1, respectively (Fig. 3e). In other words, the same flow shear velocity could suspend fewer bacteria from PDMS surfaces of lower crosslinking degree. Since the dominant contribution to detach the bacteria from the PDMS surfaces as identified in the simulation was interfacial adhesion force derived from interfacial physicochemistry, the calculated varying critical shear velocity and residual resistant torques were impacted mainly by the interfacial physicochemistry. More importantly, the experimental results of the variant residual bacterial numbers (Fig. 3 a&b) displayed a similar trend to that found in our previous report [1], which matched well with our simulation assumptions and results presented here

We further utilized COMSOL Multiphysics 5.6 to simulate the attachment and detachment process in the 3D environment (Fig. 4, Video 1–4). Particle flow (360 particles per minute in order to simulate a bacterial flow in the range of 10^2-10^3 cells per min-

Fig. 2. Bacterial attachment analysis in the attachment process. (a) and (b) depict the number of adhered *E. coli* cells on PDMS samples during the attachment processand the corresponding representative micrographs, respectively. The bacteria in PBS were flown through PDMS samples for 2 h at a speed of 100 μL·min^{-1} at room temperature, followed by flowing PBS buffer (100 μL·min^{-1}) for 15 min to remove the unattached bacteria. Attached bacteria were then imaged by optical microscopy and counted. Two replicates of each PDMS sample type were analyzed and five images at random locations were taken on each replicate. Three independent experiments were performed and one set of results was displayed. Error bars representing the standard deviations were derived based on total 10 measurements in one set of experiment. Scale bar: 50 μm. Student's *t*-test ($p < 0.01$) in (a) suggested no significant difference for every sample type. Interaction free energy (c) between a bacterial cell and different PDMS surfaces was calculated based on XDLVO model. The total interaction energy (E_TOT), the acid-basic interaction energy (E_AB), the electrostatic double layer interaction energy (E_EL), and the Lifshitz-Van der Waals interaction energy (E_LW) were calculated against the separation distance of a bacterium from different PDMS surfaces. Bacterial adhesion on different PDMS surfaces in a simulated velocity field (d) was analyzed by XDLVO model modulated in COMSOL Multiphysics 5.6. The geometry of flowing chamber was defined as 75 mm (length) × 25 mm (width) × 1 mm (height) and laminar flow (100 μL min^{-1}) in the velocity field was generated according to the compressible model ($Ma < 0.3$) and by considering the acid-base interaction, electrostatic double layer interaction, Lifshitz-Van der Waals interaction and Brownian interaction. The partial chamber (25 mm in length) was illustrated for a straightforward understanding. The bacterial trajectory and position in the simulation were depicted as particles at a mass flow rate of 0.3 mg·s^{-1} traced in fluidic flow on different PDMS surfaces. Blue dots on the bottom boundaries illustrated attached bacteria and the cone shaped velocity gradient inside the flow chamber is presented in the rainbow bar below. (For interpretation of the references to colour in this figure legend, the reader is referred to the web version of this article.)

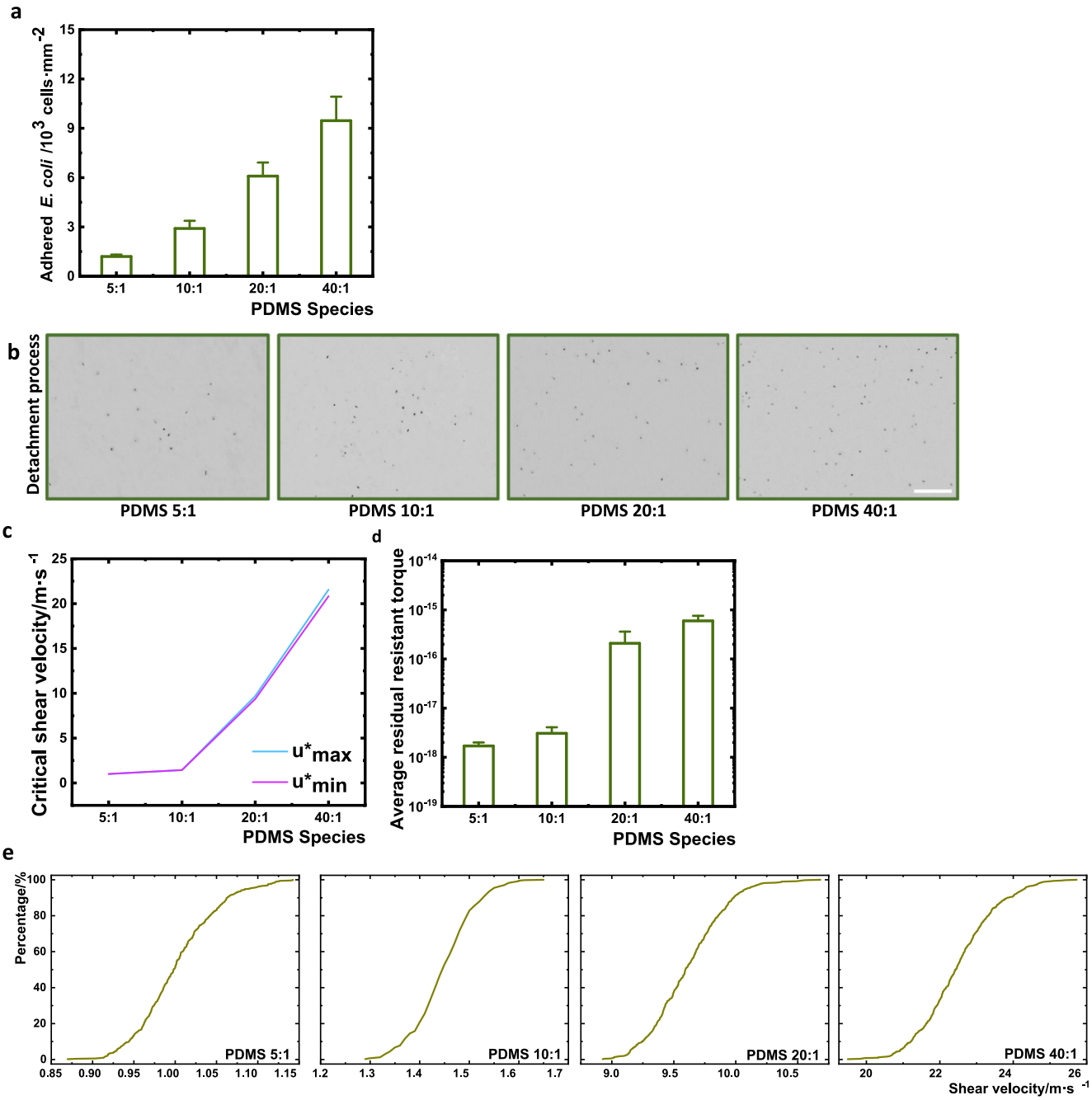

Fig. 3. Residual bacterial adhesion analysis in the detachment process. (a) and (b) illustrate the residual adhesion of *E. coli* BW25113 on PDMS samples during detachment process and the corresponding representative micrographs, respectively. The bacteria were allowed to detach from PDMS samples for 5 min by flowing air (1000 mbar) at room temperature, followed by flowing PBS buffer (100 μL·min^{-1}) for 10 min to obtain a stable status of adhered bacteria. Subsequently, the adhered bacteria were imaged by optical microscopy and counted. Two replicates of each PDMS samples were analyzed and five images at random locations were taken on each replicate. Three independent experiments were performed and one set of results is displayed. Error bars representing the standard deviations were derived based on total 10 measurements in one set of experiment. Scale bar: 50 μm. Student's *t*-test ($p < 0.01$) in (a) suggested significant difference among each sample. The mean critical shear velocities on different PDMS surfaces (c) were calculated based on Monte-Carlo simulation with defined turbulence factor and required assumed Re number. The mean critical shear velocities to suspend a bacterium on PDMS 5:1 and 10:1 were derived based on the sublayer model (assumed $Re \ll 1$) with a fixed turbulence factor of 1.14 and the ones on PDMS 20:1 and 40:1 were calculated according to the burst model (assumed $1 \leq R \leq 1000$) with a turbulence range of 1.72–1.84. Thus, fixed mean critical shear velocities can be calculated for PDMS 5:1 and 10:1 and mean critical shear velocity ranges can be derived for PDMS 20:1 and 40:1. The average residual resistant torques in a unit of N·m (d) were determined based on the resistant torques formed on PDMS surfaces once bacteria attached on a PDMS surface and torques of a flow from the detachment flow in the chamber. Thereby, the residual resistant torques indicated the resistant torques of adhered bacteria on surfaces unable to be surmounted by the flow. The number of suspended bacteria on different PDMS surface at varying shear velocities of a flow (e) were calculated based on Monte-Carlo simulation due to the surface imperfect homogeneity, uneven bacterial distribution and flow variation.

ute) was set in a simplified chamber (75 mm (length) × 12.5 mm (width) × 1 mm (height)) to interact various PDMS surfaces. The particle number above each PDMS samples (including suspended and attached particles) was counted during simulated attachment (0–120 min) and detachment (120–135 min) settings, corresponding to the aforementioned experimental settings (Fig. 4a, Video 1–4). In addition, the particles above PDMS surfaces at 120 min and 135 min were depicted, as shown in Fig. S4 a&b. It was observed

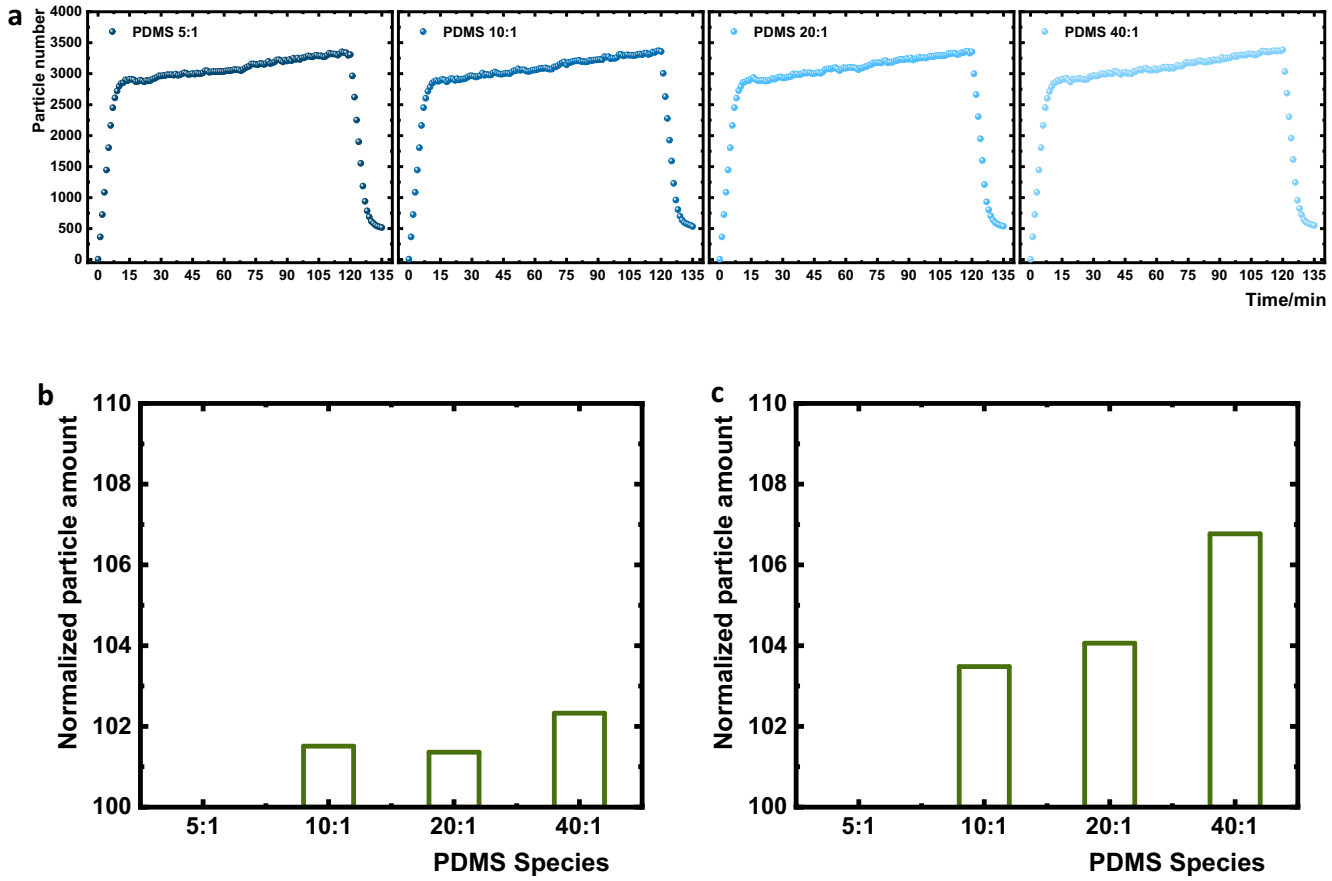

Fig. 4. Theoretical verification of a bacterial flow on various PDMS surfaces analyzed by COMSOL Multiphysics 5.6. (a) Particle number above various PDMS surfaces was recorded from 0 to 135 min, with the period of 0–120 min to simulate the attachment process and that of 120–135 min the detachment process. The particle flow was set at 360 particles per minute in a simplified chamber (75 mm (length) × 12.5 mm (width) × 1 mm (height)). (b) and (c) show the particle amounts on different PDMS surfaces at 120 min and 135 min, respectively, normalized to the number of particles above PDMS 5:1 at each time point.

that the particle number above each PDMS surface became stable after a flow for approximately 10 min (Fig. 4a), which lasted until the end of the attachment process. Only a slight variation (below 2.3%) in particle number above different PDMS surfaces can be observed at 120 min (Fig. 4b). However, this variation increased up to 6.8% after detachment at 135 min (Fig. 4c). Even though the setting of this theoretical verification was simplified, a similar trend has been observed in the 2D analysis of bacterial attachment and detachment.

These results revealed that the interfacial physicochemistry regulating the surface energy barrier dominated the residual resistant torques during the detachment, likely through molecular bridging of the non-crosslinked PDMS chains (Fig. 1b-e). Thus, it is hypothesized that interfacial physicochemistry is the regulating factor for bacterial residual adhesion behavior on PDMS surfaces.

2.4. Empirical verification through extracted-PDMS and measurement of single cell adhesion forces

In order to verify the impact of interfacial physicochemistry on residual bacterial numbers after the detachment process, we aimed to obtain PDMS substrates of comparable surface physicochemistry. To this end, we extracted the PDMS samples to remove the non-crosslinked polymer chains using the previously reported method [32]. The surface wettability of the PDMS samples was subsequently analyzed by water contact angle measurement, revealing a narrow range of 109.6 to 111.6° (Fig. 5a), unlike the different values obtained for the non-extracted PDMS samples (108.4 – 122.4°, Fig. S2c). The adhesion force (0.8 – 25.1 N) and energy (0.1 – 9.2 J·m^{-2}) of the extracted bulk PDMS measured by rheometry were considerably reduced compared to those before extraction (Fig. 5 b&c). However, the sample 40:1 still exhibited highest bulk adhesion force and bulk energy, and the sample 5:1 the lowest. As expected, the stiffness (shear complex modulus) of all samples after extraction increased dramatically upon removal of non-crosslinked polymer chains, from 69 to 7385 kPa for sample 5:1 and from 4 to 2422 kPa for sample 40:1 (Fig. S1, Table 1). Nevertheless, 5:1 remained the stiffest and 40:1 the softest material (Fig. S1). The interfacial Young's modulus measured by AFM demonstrated a rising trend similar to the bulk shear modulus, from 2401 to 3490 kPa for extracted PDMS 5:1 and from 66 to 206 kPa for extracted PDMS 40:1 (Fig. 5d). The roughness (Rq) on different PDMS surfaces after extraction was reduced to the range of 1.8 to 4.6 nm (Fig. 5e), differing from the non-extracted PDMS surfaces (ranging of 1.8 to 9.2 nm, Fig. S2d). The interfacial adhesion force, 1.87 to 4.98 nN, displayed no significant difference for the extracted PDMS samples of varying crosslinking degrees (Fig. 5f), indicating that the non-crosslinked PDMS polymer chains were removed from the PDMS samples. This was further proved by single cell force spectroscopy through FluidFM. For PDMS 5:1, 10:1, 20:1 and 40:1, the average adhesion forces between a bacterium and non-extracted PDMS surfaces were 3.0 nN, 38.1 nN, 105.8 nN and 247.2 nN, respectively, displaying a significant difference according to Student's *t*-test ($p < 0.01$). On the contrary, the aver-

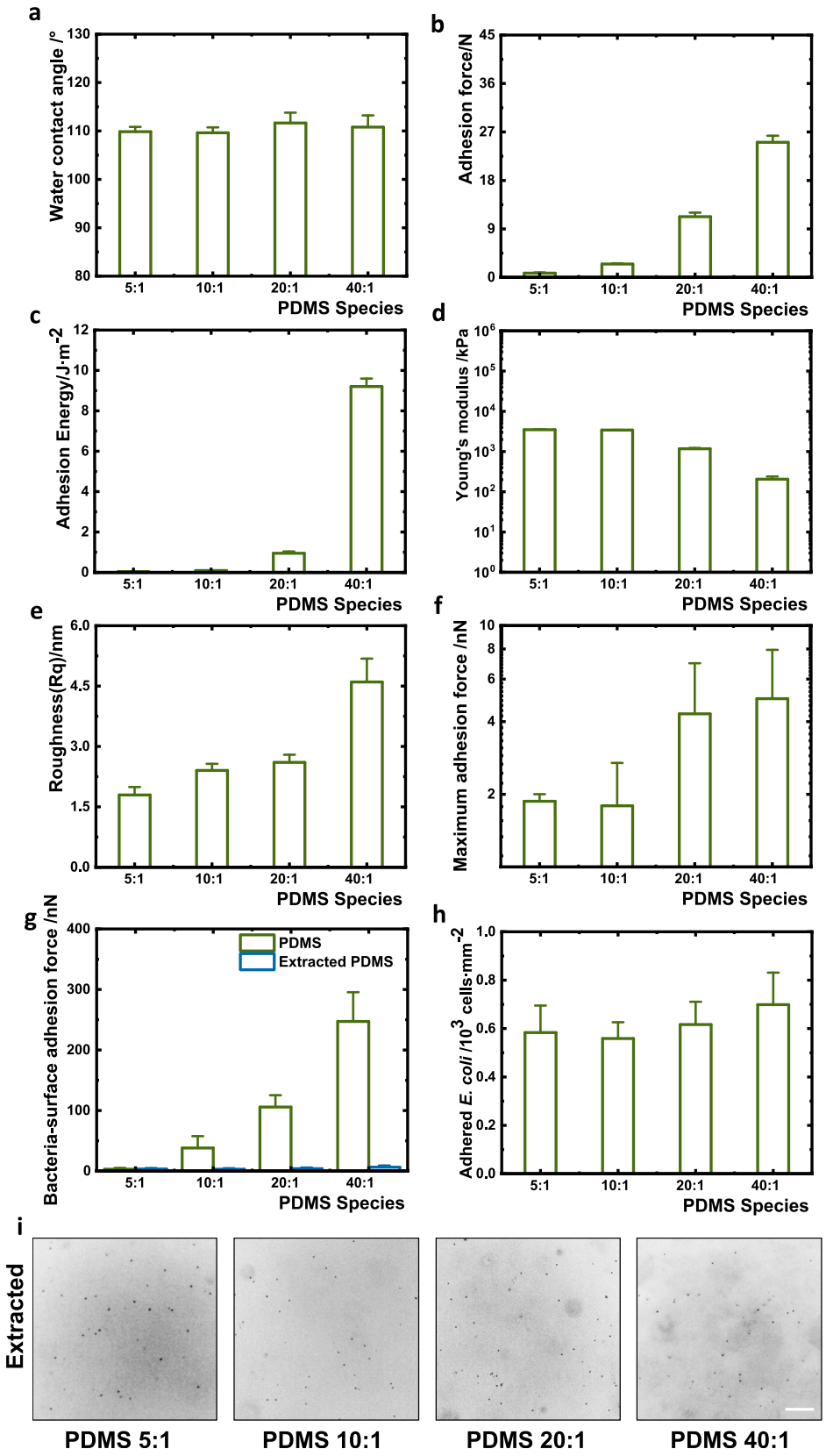
a
Water contact angle /°
130
120
110
100
90
80
5:1
10:1
20:1
40:1
PDMS Species
b
Adhesion force/N
45
36
27
18
9
0
5:1
10:1
20:1
40:1
PDMS Species
c
Adhesion Energy/J·m-2
12
10
8
6
4
2
0
5:1
10:1
20:1
40:1
PDMS Species
d
Young's modulus /kPa
10^6
10^5
10^4
10^3
10^2
10^1
10^0
5:1
10:1
20:1
40:1
PDMS Species
e
Roughness(Rq)/nm
6.0
4.5
3.0
1.5
0.0
5:1
10:1
20:1
40:1
PDMS Species
f
Maximum adhesion force /nN
10
8
6
4
2
5:1
10:1
20:1
40:1
PDMS Species
g
Bacteria-surface adhesion force /nN
400
300
200
100
0
PDMS
Extracted PDMS
5:1
10:1
20:1
40:1
PDMS Species
h
Adhered E. coli /10^3 cells·mm-2
1.0
0.8
0.6
0.4
0.2
0.0
5:1
10:1
20:1
40:1
PDMS Species
i
Extracted
PDMS 5:1
PDMS 10:1
PDMS 20:1
PDMS 40:1

age adhesion forces between a bacterium and extracted PDMS surfaces were respectively 3.4 nN, 3.0 nN, 4.0 nN and 6.4 nN, showing no significant difference according to Student's *t*-test. As expected, the numbers of adhered bacteria on different extracted PDMS surfaces were found to be similar (Fig. 5 h&i). The analysis through single cell force spectroscopy herewith provided us a direct empirical evidence that surface physicochemistry of PDMS played a decisive role in bacterial adhesion forces and the residual resistant torques, and consequently the residual bacterial adhesion.

Hence the variable surface physicochemistry of PDMS samples caused by varying crosslinking degree was attributed to different amount of free PMDS chains and different length of chain ends on surfaces, referring to our precedent work [1]. However, such variation does not affect bacterial adhesion on different PDMS surfaces during the bacterial attachment process since the tested PDMS surfaces confer a comparable energy barrier of 500 k_BT for their interaction with bacteria. In contrast to the bacterial attachment process, a detachment process led to varying residual numbers of bacteria on PDMS surfaces, which is in agreement with the calculated varying critical shear velocity and residual resistant torques, mainly impacted by the interfacial physicochemistry. After extraction of the non-crosslinked PDMS polymer chains, the interfacial mechanical properties of different PDMS remained different, but the interfacial maximum adhesion forces of the extracted samples were similar, indicating a similar interfacial physicochemical property of PDMS surfaces after extraction. Moreover, the extracted PDMS samples permitted similar numbers of adhered bacteria, alongside comparable bacterium adhesion forces. We therefore speculate that bacteria that are loosely attached on different PDMS surfaces during the bacterial attachment phase can be flushed away in the detachment process. The different interfacial physicochemistry determined by the amount of free/non-crosslinked PDMS polymer chains [33] worked therefore as interfacial "glue" of variable binding strength to allow different numbers of adhered residual bacteria after a rigorous detachment process, revealed by the final residual bacteria on PMDS. Hence interfacial physicochemistry, as hypothesized, was confirmed to regulate the bacterial interaction with PDMS surfaces during the attachment and the detachment process.

In this work, we idealized bacteria as homogenous spherical particles and utilized PBS to suspend bacterial cells to simplify the interaction of bacteria and surfaces. In the future, it is necessary to further study more complex systems, for example investigating how a nutrient-containing medium would influence the bacteria-surface interaction since biomolecules e.g., proteins in the medium could be absorbed differently by PDMS with different physicochemistry, thus impact the subsequent bacterial adhesion.

3. Conclusions

Based on both empirical and simulation studies of bacterial attachment and detachment, we noticed that the identical energy barrier of different PDMS surfaces resulted in a similar number of bacteria attached on these surfaces during the attachment process. The residual bacterial adhesion on different PDMS surfaces increased with decreasing degree of polymer crosslinking in the PDMS samples. In addition, the observed residual bacterial adhesion after detachment was in accordance with an increasing critical shear velocity and residual resistant torques. The different critical shear velocities and residual resistant torques based on simulation setting are originated from the different interfacial physicochemistry of the PDMS materials. The dominant influence of interfacial physicochemistry on residual bacterial adhesion was also verified by the utilization of the extracted PDMS samples and by direct measurement of the interactions with FluidFM. The surface binding strength of bacteria was also revealed to be dependent on the interfacial physicochemistry. This comprehension of bacterial interaction with materials surfaces assisted by theoretical simulation and empirical analysis facilitates the interpretation of bacterial interaction with materials and provides insights into parameters to further improve the design of bio-functional materials surfaces.

4. Methods

4.1. Empirical analysis

Chemical and reagents. All chemicals and reagents were purchased from Sigma-Aldrich (Buchs, Switzerland) and utilized as received unless otherwise stated. Phosphate-buffered saline (PBS) at pH 7.4 was prepared as following: 8 $g{\cdot}L^{-1}$ NaCl, 0.2 $g{\cdot}L^{-1}$ KH_2PO_4 and 1.44 $g{\cdot}L^{-1}$ Na_2PO_4 in distilled water. Bacterial growth medium (LB broth) was prepared as following: 10 $g{\cdot}L^{-1}$ tryptone, 5 $g{\cdot}L^{-1}$ yeast extract and 5 $g{\cdot}L^{-1}$ NaCl in distilled water.

PDMS substrate preparation. PDMS substrates were prepared as previously reported using a Sylgard184 silicone elastomer kit (Dow corning Inc., USA) with different weight ratios of the curing agent of 5:1, 10:1, 20:1 and 40:1 [1,13]. The mixtures were thoroughly mixed, degassed in vacuum for 30 min and subsequently 20 μL PDMS were pipetted into 8-well slides as shown in Fig. S5a to eliminate the position influence on bacterial adhesion. Then all prepared slides were located on horizontally levelled racks inside a vacuum incubator (SalvisLab Vacucenter, Switzerland) in vacuum (blew 0.1 mbar) for half an hour and then kept at 60 °C for 24 h after vacuum release. All fabricated slides were immersed in 70%

Fig. 5. Surface and bulk characterization of extracted PDMS samples and single cell adhesion force analysis of non-extracted and extracted PDMS samples. Water contact angle measurements (a) were performed with five replicates of every PDMS species and every replicate was measured six times. The error bars were respectively calculated based on 30 measurements. Bulk adhesion force (b) and adhesion energy (c) of extracted PDMS were analyzed using a rheometer with three independent measurements in triplicate. Young's modulus (d), surface average roughness (e) and maximum surface adhesion force (f) were measured in PBS buffer by AFM. Three replicates of every PDMS species were measured by AFM-force spectroscopy and 576 indentations of every replicate were performed to derive surface Young's modulus (d) and adhesion force (f), and the related standard deviation. Surface average roughness (Rq) (e) was measured in PBS buffer by AFM contact mode. The samples were measured in triplicate and each replicate was analyzed five times to derive error bars. Single cell adhesion forces between an *E. coli* bacterium and every sample surface (g) was analyzed in PBS buffer by Fluidic FM and 10 measurements for every sample were conducted. Adhesion of *E. coli* was analyzed on extracted PDMS samples (h) alongside with corresponding representative micrographs of adhered *E. coli* on extracted PDMS surfaces (i). The bacteria were incubated with extracted PDMS samples for 2 h in PBS, followed by careful removal of the suspensions. Every sample was subsequently rinsed carefully with fresh PBS twice to remove non-attached bacteria. Adhered bacteria were then imaged by optical microscopy and counted. Three replicates of every PDMS species were analyzed and five images at random locations were taken on every replicate. Three independent experiments were performed and one set of results is displayed here. Error bars representing the standard deviations were derived based on total 15 measurements in one set of experiment. Scale bar: 50 μm. Student's *t*-test ($p < 0.01$) in (a), (f), (g) and (h) revealed no significant difference among extracted samples but suggested significant difference among extracted samples in (b), (c), (d) and (e) and among non-extracted samples in (g).

ethanol for 20 min for cleaning and subsequently dried in vacuum before further experiments unless otherwise stated.

Water contact angle measurement. The contact angle was analyzed by a Drop Shape Analyzer DSA25E (Krüss GmbH, Germany). The contact angle was measured on PDMS surfaces with deionized water, formamide and ethylene glycol (Table S1). The measurements were performed at least five times on random positions of one PMDS substrate with three replicates.

Atomic force microscope (AFM) analysis. AFM characterization was performed on PDMS surfaces (punched discs with a diameter of 20 mm) in PBS by a Flex Bio-AFM (Nanosurf, Switzerland). Surface topography and force curve measurement were conducted with a cantilever PointProbe® Plus Non-Contact / Soft Tapping Mode - Au Coating (PPP-NCST-Au, Nanosensor, Switzerland). Elastic deformation of PDMS substrates was used to derive Young's modulus from AFM-force spectroscopy by AtomicJ converting raw deflection vs sample displacements plots into force vs deformation plots based on the probe signal sensitivity ($nm \cdot V^{-1}$) and spring constant ($N \cdot m^{-1}$) [1,34-36].

Free-PDMS extraction from bulk substrates. Extraction of non-crosslinked PDMS polymer chains was performed as previously reported [32]. Briefly, the PDMS samples of different cross-linking degree were sequentially extracted by pentane for two days, allowed to dwell in toluene for one day, ethyl acetate for one day and acetone for one day, and finally dried in an oven at 90 °C for two days.

Gel fraction determination. The gel fraction was analyzed as reported [1]. The mass of PDMS samples (punched discs with a diameter of 20 mm) was measured before free-PDMS extraction (W_1) and after (W_2) as described above. The gel fraction was then derived as following:

$$Gel\ fraction = W_2/W_1 \times 100\%$$

Rheology characterization. Rheological properties of PDMS substrates (all substrates were punched into discs with diameter of 20 mm) were measured [1] by *in situ* plate-to-plate rheometer (Anton-Paar 301, Graz). PDMS discs were placed on the bottom plate and tool master was located above the substrate surface. (1) Time-sweep measurements were performed with a constant angular frequency of 10 $rad \cdot s^{-1}$ and strain of 0.5% for the punched PDMS substrates. Shear complex modulus was consequently calculated as:

$$|G^*| = \sqrt{G'^2 + G''^2}$$

G* is shear complex modulus, G' is storage modulus and G" is loss modulus.

(2) In the adhesion force measurement, the samples were located at the center of the bottom plate and the rheometer upper plate was lowered to the samples until physical contact. Each sample was loaded with a constant normal force (F_N) of 10 N by the upper plate for 5 s. The upper plate was then programmed to move upwards with a speed of 5 $mm \cdot s^{-1}$ until a desired gap distance (h) of 30 mm was reached. The measured normal forces were analyzed against gap distance. F_N against gap distance was integrated by Origin 2019 to derive the adhesion energy of each sample with the upper plate.

Bacteria culture. E. coli BW25113, a strain widely utilized for biofilm research [37,38], was used in this work. A bacteria colony was picked from an agar plate, incubated in 10 mL LB growth medium in a 50 mL Falcon tube on an orbital shaker at 160 rpm at 37 °C. 1 mL overnight bacterial culture was transferred into a 10 mL fresh LB growth medium and then cultivated in the same shaker for about 2 h till its exponential growth phase. Subsequently the bacterial culture was centrifuged at 7500 rpm for 5 min at 4 °C and washed three times with 10 mL PBS.

Bacterial attachment and detachment assay. The configuration of the flow system to perform bacterial attachment and detachment assay is described in Fig. S5b [13]. After the 8-well slide with PDMS samples was assembled in the flow chamber (height 1 mm, width 25 mm and length 75 mm, Fig. S5b(8)), 70% ethanol was utilized to disinfect all components by circuiting the system for 15 min at a speed of 100 $\mu L \cdot min^{-1}$ using a flow controller (OB1 pressure controller, Elveflow, France). Subsequently PBS was perfused into the system for 15 min at a flow of 100 $\mu L \cdot min^{-1}$ to condition the PDMS samples. The bacterial suspension (diluted to OD_{600} 0.01) was subjected to a flow over the PDMS sample for 120 min at a speed of 100 $\mu L \cdot min^{-1}$. Then the bacterial suspension was replaced by PBS to flow for 15 min with the same speed and air was also subsequently utilized to flow in the chamber for 5 min at a controlled pressure of 1000 mbar in order to remove bacteria [13]. Finally, PBS was perfused in the chamber for 10 min at a speed of 100 $\mu L \cdot min^{-1}$ to keep bacteria in liquid condition. Bacterial adhesion was visualized by optical microscopy (DM6000B, Leica, Switzerland) equipped with a 40x objective (ULWD 0.50 160/0-2. Olympus, Japan). Adhered bacteria were imaged randomly at three different locations (area of each location: 0.0069 mm^2) for every sample species and three independent experiments were performed. All the components in the fluidic system were connected by polytetrafluoroethylene tubes (with an inner diameter of 0.5 mm, (Bola S1810-09, BOHLENDER, Germany)) and autoclaved before experiments.

Bacterial adhesion on extracted PDMS samples. The bacterial adhesion assays were performed as reported previously [1,12,13]. Extracted PDMS samples were cut into discs with a diameter of 20 mm and placed in 12 well plates (TPP, Switzerland). All samples were sterilized with 2 mL 70% ethanol for 20 min and then immersed in 2 mL PBS for 2 h for stabilization. The cultures of bacteria of exponential growth in LB were centrifuged at 7500 rpm for 5 min at 4 °C and washed with 10 mL PBS buffer three times. The bacterial cells were subsequently re-suspended in PBS buffer to reach 2×10^6 colony forming units (CFU)$\cdot mL^{-1}$. 1.5 mL of bacterial suspension were added to every well and all samples were incubated for 2 h. Bacterial suspension was carefully removed after incubation and all samples were gently rinsed with 2 mL fresh PBS buffer twice to remove non-adhered bacterial cells.

Quantification of adhered bacteria. Samples with adhering bacteria were first treated with fixation solution (4% paraformaldehyde and 2.5% glutaraldehyde) for half an hour and afterwards immersed in surface passivation solution containing 0.1% bovine serum albumin for 5 min. The bacteria adhered to the extracted-PDMS surfaces were analyzed by optical microscopy (Inverted microscope Eclipse Ti2E (Nikon, Japan) equipped with a 40X objective lens) .

FluidFM setup. A Flex Bio-AFM (Nanosurf, Switzerland) and a digital pressure controller (Cytosurge, Switzerland) were utilized, as adapted from the previous report [20], together with an AxioObserver Z1 inverted microscope (Carl Zeiss, Germany) to ensure an optical control throughout the measurements. FluidFM nanopipettes with a nominal spring constant of 2 $N \cdot m^{-1}$ (Cytosurge, Switzerland) were utilized for bacterial adhesion measurements. The cantilevers were plasma treated for 30 s (Plasma Cleaner PD-32G, Harrick Plasma) and then coated with SL2 Sigmacote in order to avoid fouling. Probes were subsequently stored overnight in a desiccator, in which 1 mL Sigmacote siliconizing reagent had been poured inside beforehand, and finally dried at 100 °C for 60 min. The spring constant of cantilevers was furthermore determined in accordance to their resonance frequency in liquid by Nanosurf C3000 software (Nanosurf, Switzerland). The microchannel inside the cantilever was filled with filtered deionized water by application of pressure through the digital pressure controller. The can-

tilever sensitivity was recalibrated every time after *E. coli* bacterium remobilization on cantilevers.

Analysis of adhesion forces between bacteria and surfaces. Single cell force spectroscopy was performed at room temperature in PBS (pH 7.4) containing *E. coli*, dispersed onto a confined region of the glass dish. Cantilevers were manipulated to contact the selected *E. coli* bacterium with a force-setpoint of 10 nN. Upon contact, a negative pressure of 800 mbar was applied to reversibly immobilize single *E. coli* bacteria at the cantilever aperture. Subsequently the cantilever with a single immobilized *E. coli* bacterium was moved to a new glass dish containing a PDMS sample (diameter of 20 mm) and remained in PBS (pH 7.4). The PDMS sample was approached with the *E. coli*-probe at a speed of 1 μm s^{-1} until a force of 10 nN was measured. To confer a reproduceable interaction, this force was maintained for 5 s. The *E. coli*-probe was then retracted at a piezo velocity of 1 μm s^{-1} in the meanwhile the occurring forces was simultaneously recorded. 10 measurements were carried out for each PDMS sample and at least three different bacteria were applied for every tested PDMS sample. The adhesion forces were derived as previously reported [20] with SPIP software (Image Metrology A/S, Denmark).

4.2. Statistics

Unpaired and two-tailed Student's *t*-test were utilized in this study for statistical analysis.

4.3. Simulations

XDLVO. The total free energy of interaction between a bacterium and a PDMS surface immersed in PBS buffer was the sum of energy and the Lewis acid-base interaction energy, the repulsive electrostatic double layer interaction energy and the attractive Lifshitz-Van der Waals interaction energy. The total interaction energy calculated as a function of the separation distance was utilized by Derjaguin approximation [14]. The detailed information is provided in the supporting information S6.

The XDLVO simulations detailed in S7 were performed with COMSOL Multiphysics 5.6 to study the bacterial adhesion in the attachment process. A laminar flow (100 μL·min^{-1}) was generated based on the compressible model (Ma < 0.3) in the created geometry 75 mm (length) × 25 mm (width) × 1 mm (height) of a flow chamber, considering Lewis acid-base interaction, electrostatic double layer interaction, Lifshitz-Van der Waals interaction and Brownian interaction. The bacterial trajectory and position simulation were simplified as particles tracing at a mass flow rate of 0.3 mg·s^{-1} in fluid flow on PDMS surfaces. In the simplified simulation of particles, the particle flow was instead set to 360 particles per minute in a chamber (75 mm (length) × 12.5 mm (width) × 1 mm (height)).

Burst/sublayer model. In the burst/sublayer model [28], the bacterium was assumed as an elastic particle to contact a deformable surface with a dominating adhesion force. According to applicable conditions, it can be classified by a sublayer model and a burst model. The sublayer model as described in S8 was utilized to study the shear velocity to flush attached bacteria from different PDMS surfaces in a small fluid turbulence ($Re \ll 1$) with a fixed turbulence factor and subsequently to derive the residual resistant torque in the according flowing condition. The burst model as described in S8 was utilized to calculate the shear velocity to flush attached bacteria from different PDMS surfaces in a large fluidic turbulence ($1 \leq Re \leq 1000$) with a certain range of turbulence factor and subsequently to derive the residual resistant torque in the according flowing condition.

CRediT authorship contribution statement

Fei Pan: Conceptualization, Methodology, Software, Validation, Formal analysis, Investigation, Visualization, Supervision, Project administration, Writing – original draft, Writing – review & editing. **Mengdi Liu:** Conceptualization, Methodology, Software, Validation, Formal analysis, Investigation, Visualization, Project administration, Writing – original draft, Writing – review & editing. **Stefanie Altenried:** Methodology, Formal analysis, Validation, Investigation. **Min Lei:** Methodology, Software, Validation, Investigation, Writing – review & editing. **Jiaxin Yang:** Methodology, Software, Validation, Investigation. **Hervé Straub:** Methodology, Formal analysis, Validation, Writing – review & editing. **Wolfgang W. Schmahl:** Methodology, Validation, Supervision, Writing – review & editing. **Katharina Maniura-Weber:** Supervision, Resources, Writing – review & editing. **Orane Guillaume-Gentil:** Methodology, Formal analysis, Resources, Writing – review & editing. **Qun Ren:** Conceptualization, Methodology, Validation, Formal analysis, Investigation, Supervision, Project administration, Writing – review & editing.

Declaration of Competing Interest

The authors declare that they have no known competing financial interests or personal relationships that could have appeared to influence the work reported in this paper.

Acknowledgements

The authors thank Madeleine Ramstedt for providing the *E. coli* strain, Thijs Defraeye for support with simulation software COMSOL equipped with Multiphysics module 5.6, Henny C. van der Mei for her scientific input to this work, and Maximilian Mittelviefhaus for his valuable support in setting up the FluidFM method.

Appendix A. Supplementary data

Supplementary data to this article can be found online at https://doi.org/10.1016/j.jcis.2022.04.084.

References

[1] F. Pan, S. Altenried, M. Liu, D. Hegemann, E. Bülbül, J. Moeller, W.W. Schmahl, K. Maniura-Weber, Q. Ren, A nanolayer coating on polydimethylsiloxane surfaces enables a mechanistic study of bacterial adhesion influenced by material surface physicochemistry, Mater. Horizons 7 (1) (2020) 93–103.
[2] F. Pan, A. Amarjargal, S. Altenried, M. Liu, F. Zuber, Z. Zeng, R.M. Rossi, K. Maniura-Weber, Q. Ren, Bioresponsive hybrid nanofibers enable controlled drug delivery through glass transition switching at physiological temperature, ACS Appl. Bio Mater. 4 (5) (2021) 4271–4279.
[3] A. Milionis, A. Tripathy, M. Donati, C.S. Sharma, F. Pan, K. Maniura-Weber, Q. Ren, D. Poulikakos, Water-based scalable methods for self-cleaning antibacterial ZnO-nanostructured surfaces, Ind. Eng. Chem. Res. 59 (32) (2020) 14323–14333.
[4] F. Pan, S. Altenried, F. Zuber, R.S. Wagner, Y.-H. Su, M. Rottmar, K. Maniura-Weber, Q. Ren, Photo-activated titanium surface confers time dependent bactericidal activity towards Gram positive and negative bacteria, Colloids Surf., B 206 (2021) 111940, https://doi.org/10.1016/j.colsurfb.2021.111940.
[5] F. Song, M.E. Brasch, H. Wang, J.H. Henderson, K. Sauer, D. Ren, How bacteria respond to material stiffness during attachment: a role of Escherichia coli flagellar motility, ACS Appl. Mater. Interfaces 9 (27) (2017) 22176–22184.
[6] N. Saha, C. Monge, V. Dulong, C. Picart, K. Glinel, Influence of polyelectrolyte film stiffness on bacterial growth, Biomacromolecules 14 (2) (2013) 520–528.
[7] J.A. Lichter, M.T. Thompson, M. Delgadillo, T. Nishikawa, M.F. Rubner, K.J. Van Vliet, Substrata mechanical stiffness can regulate adhesion of viable bacteria, Biomacromolecules 9 (6) (2008) 1571–1578.
[8] D.P. Bakker, F.M. Huijs, J. de Vries, J.W. Klijnstra, H.J. Busscher, H.C. van der Mei, Bacterial deposition to fluoridated and non-fluoridated polyurethane coatings with different elastic modulus and surface tension in a parallel plate and a stagnation point flow chamber, Colloids Surf., B 32 (3) (2003) 179–190.

[9] C. Guégan, J. Garderes, G. Le Pennec, F. Gaillard, F. Fay, I. Linossier, J.-M. Herry, M.-N.-B. Fontaine, K.V. Réhel, Alteration of bacterial adhesion induced by the substrate stiffness, Colloids Surf., B 114 (2014) 193–200.
[10] K.W. Kolewe, S.R. Peyton, J.D. Schiffman, Fewer bacteria adhere to softer hydrogels, ACS Appl. Mater. Interfaces 7 (35) (2015) 19562–19569.
[11] K.W. Kolewe, J. Zhu, N.R. Mako, S.S. Nonnenmann, J.D. Schiffman, Bacterial adhesion is affected by the thickness and stiffness of poly(ethylene glycol) hydrogels, ACS Appl. Mater. Interfaces 10 (3) (2018) 2275–2281.
[12] H. Straub, C.M. Bigger, J. Valentin, D. Abt, X.-H. Qin, L. Eberl, K. Maniura-Weber, Q. Ren, Bacterial adhesion on soft materials: passive physicochemical interactions or active bacterial mechanosensing?, Adv Healthcare Mater. 8 (8) (2019) 1801323, https://doi.org/10.1002/adhm.v8.810.1002/adhm.201801323.
[13] J.D.P. Valentin, X.-H. Qin, C. Fessele, H. Straub, H.C. van der Mei, M.T. Buhmann, K. Maniura-Weber, Q. Ren, Substrate viscosity plays an important role in bacterial adhesion under fluid flow, J. Colloid Interface Sci. 552 (2019) 247–257.
[14] S. Wu, S. Altenried, A. Zogg, F. Zuber, K. Maniura-Weber, Q. Ren, Role of the surface nanoscale roughness of stainless steel on bacterial adhesion and microcolony formation, ACS Omega 3 (6) (2018) 6456–6464.
[15] N.P. Boks, W. Norde, H.C. van der Mei, H.J. Busscher, Forces involved in bacterial adhesion to hydrophilic and hydrophobic surfaces, Microbiology 154 (10) (2008) 3122–3133.
[16] F.-G. Fan, G. Ahmadi, A sublayer model for turbulent deposition of particles in vertical ducts with smooth and rough surfaces, J. Aerosol Sci. 24 (1) (1993) 45–64.
[17] C.-J. Tsai, D.Y.H. Pui, B.Y.H. Liu, Elastic flattening and particle adhesion, Aerosol Sci. Technol. 15 (4) (1991) 239–255.
[18] W.C. Hinds, Aerosol technology: properties, behavior, and measurement of airborne particles, John Wiley & Sons, 1999.
[19] O. Guillaume-Gentil, M. Mittelviefhaus, L. Dorwling-Carter, T. Zambelli, J.A. Vorholt, FluidFM applications in single-cell biology, in: E. Delamarche, G.V. Kaigala (Eds.), Open-Space Microfluidics: Concepts, Implementations, Applications: Concepts, Implementations, Applications, Wiley-VCH Verlag GmbH & Co. KGaA, Weinheim, Germany, 2018, pp. 325–354, https://doi.org/10.1002/9783527696789.ch15.
[20] M. Mittelviefhaus, D.B. Müller, T. Zambelli, J.A. Vorholt, A modular atomic force microscopy approach reveals a large range of hydrophobic adhesion forces among bacterial members of the leaf microbiota, ISME J. 13 (7) (2019) 1878–1882.
[21] C. Gómez-Suárez, H.J. Busscher, H.C. van der Mei, Analysis of bacterial detachment from substratum surfaces by the passage of air-liquid interfaces, Appl. Environ. Microbiol. 67 (6) (2001) 2531–2537.
[22] K.C. Marshall, R. Stout, R. Mitchell, Mechanism of the initial events in the sorption of marine bacteria to surfaces, Microbiol. 68 (3) (1971) 337–348.
[23] R.M. Fitch, Principles of colloid and surface chemistry, by Paul C. Hiemenz, Marcel Dekker, New York, 1977, 516 pp. No Price given, J. Polym. Sci. B Polym. Lett. Ed. 22 (9) (1984) 508–509, https://doi.org/10.1002/pol.1984.130220910.
[24] K. Hori, S. Matsumoto, Bacterial adhesion: From mechanism to control, Biochem Eng J. 48 (3) (2010) 424–434.
[25] C.J. Van Oss, The forces involved in bioadhesion to flat surfaces and particles — Their determination and relative roles, Biofouling 4 (1-3) (1991) 25–35.
[26] C.J. van Oss, M.K. Chaudhury, R.J. Good, Monopolar surfaces, Adv. Colloid Interface Sci. 28 (1987) 35–64.
[27] R. Bos, H.C. van der Mei, H.J. Busscher, Physico-chemistry of initial microbial adhesive interactions – its mechanisms and methods for study, FEMS Microbiol Rev. 23 (2) (1999) 179–230.
[28] M. Soltani, G. Ahmadi, R.G. Bayer, M.A. Gaynes, Particle detachment mechanisms from rough surfaces under substrate acceleration, J. Adhes. Sci. Technol. 9 (4) (1995) 453–473.
[29] K.L. Johnson, K. Kendall, A. Roberts, Surface energy and the contact of elastic solids, Proc. Roy. Soc. London. A. Math. Phys. Sci. 324 (1558) (1971) 301–313.
[30] G. Ahmadi, S. Guo, Bumpy particle adhesion and removal in turbulent flows including electrostatic and capillary forces, J. Adhesion 83 (3) (2007) 289–311.
[31] D.M. Benov, The Manhattan Project, the first electronic computer and the Monte Carlo method, Monte Carlo Methods Appl. 22 (1) (2016) 73–79.
[32] J.N. Lee, C. Park, G.M. Whitesides, Solvent compatibility of poly (dimethylsiloxane)-based microfluidic devices, Anal. Chem. 75 (23) (2003) 6544–6554.
[33] J.J. Sahlin, N.A. Peppas, Enhanced hydrogel adhesion by polymer interdiffusion: use of linear poly (ethylene glycol) as an adhesion promoter, J. Biomater. Sci. Polym. Ed. 8 (6) (1997) 421–436.
[34] P. Hermanowicz, M. Sarna, K. Burda, H. Gabryś, AtomicJ: an open source software for analysis of force curves, Rev. Sci. Instrum. 85 (6) (2014) 063703, https://doi.org/10.1063/1.4881683.
[35] K. Gotlib-Vainshtein, O. Girshevitz, C.N. Sukenik, D. Barlam, E. Kalfon-Cohen, S. R. Cohen, Oxide surfaces with tunable stiffness, J. Phys. Chem. C 117 (43) (2013) 22232–22239.
[36] A.C. Chang, B.H. Liu, Modified flat-punch model for hyperelastic polymeric and biological materials in nanoindentation, Mech. Mater. 118 (2018) 17–21.
[37] T.K. Wood, Insights on Escherichia coli biofilm formation and inhibition from whole-transcriptome profiling, Environ. Microbiol. 11 (1) (2009) 1–15.
[38] J. Zhao, Q. Wang, M. Li, B.D. Heijstra, S. Wang, Q. Liang, Q. Qi, Escherichia coli toxin gene hipA affects biofilm formation and DNA release, Microbiology 159 (3) (2013) 633–640.